Chapter 15
Influence of Laser Speed and Power on the Magnetic Properties of Fe-50 Wt% Ni Alloy Manufactured by LPBF

C. Guerra, J. Ramos-Grez, Rossi Setchi, P. Anderson, M. Biyiklioglu, and I. La Fe

Abstract Soft magnetic materials are used in a wide range of devices, including mobile phones, computers, motors, and inductors. Among the soft magnets, the Fe-50 wt% Ni alloy exhibits superior properties such as high magnetic saturation and permeability with low coercivity, when manufactured by conventional methods such as injection moulding. However, until now, it is not clear if modern manufacturing methods such as those based on laser powder bed fusion can affect the magnetic response. This work aims to determine experimentally the influence of laser speed and power through additive manufacture and subsequent magnetic characterization of the manufactured samples. These measurements were compared with those of a commercial sample obtained via conventional fabrication methods. The results show that it is possible to achieve magnetic saturation similar to the commercial samples, with both values of ~1.7 T and acceptable permeability of 66 A·m^{-1} compared to the commercial ones 159 A·m^{-1} if samples were fabricated with 190 W laser power and 300 m·s^{-1} laser speed.

15.1 Introduction

Soft magnetic materials, such as Fe–Si, Fe–Ni, Fe–Al–Si, and Fe–Co to name some, are widely used in modern electric and electronic devices [1, 2]. They transform electrical to mechanical energy and are indispensable in applications that involve the conversion of the electric current waveform. Therefore, their application includes transformers, inductors, communication equipment such as audio transformers,

C. Guerra (✉) · J. Ramos-Grez · I. La Fe
Escuela de Ingeniería, Pontificia Universidad Católica de Chile, Av. Vicuña Mackenna, 4860 Macul, Santiago, Chile
e-mail: caguerra2@uc.cl

R. Setchi · P. Anderson · M. Biyiklioglu
Cardiff School of Engineering, The Parade, Cardiff CF24 3AA, UK

recording heads and magnetic modulators and are widely used in ordinary appliances such as hair dryers, vacuum cleaners, washing machines, air conditioners, phone (wireless) chargers, and computer power supplies [3].

A soft magnetic material is characterized by very high magnetic permeability, low coercivity, and high magnetic saturation [4]. In practice, it is visualized on a hysteresis loop where the magnetic response shows a quasi-reversible ferromagnetic system of dipoles, whose response is nonlinear and depends on the dipoles' rotation into the field direction applied [5]. The Fe-50% Ni alloy, also called permalloy, is considered a soft magnet with a relatively high magnetic saturation (~1.6 T), high relative permeability (10,000–55,000), and low eddy current losses [5, 6]. Although it has advantages from the point of view of magnetic properties over other alloys, it is more expensive than Fe-Si.

Currently, soft magnets are fabricated through a cold rolled strip process, and in the case of brittle alloys or hard-to-work, the manufacturing process could be powder injection moulding or powder metallurgy [7, 8]. However, these techniques are limited in terms of the shape of the part that can be produced and therefore the customization of the magnets. For this reason, additive manufacturing (AM) has been suggested as an alternative for producing parts with magnetic properties [7]. Fe-50% Ni alloy has been successfully manufactured by laser powder bed fusion (LPBF) [9, 10] as well as through direct energy deposition (DED) [11, 12]. The authors have demonstrated reaching lower magnetic saturation and permeability than the alloy fabricated by other techniques, due to the presence of porosity and other defects produced during the solidification. Nevertheless, it has been observed that by increasing the grain size and applying stress relief through heat treatment, magnetic properties, such as permeability, can be enhanced in samples fabricated using AM [13]. Haftlang et al. conducted a study on Fe–Ni alloy, investigating how its crystallographic texture can facilitate the alignment of magnetic domains, thereby capitalizing on crystallographic anisotropy [12]. Additionally, Zhang et al. who produce Fe-30% Ni by LPBF discuss the laser parameters handling to achieve low crystallite size (130 µm) and then get better magnetic properties [14]. However, the influence of important process parameters such as the laser speed and power on the magnetic properties is currently unknown.

This study aims to fabricate samples using an experimental design to statistically analyse the optimal combination of laser parameters to achieve optimum magnetic properties. The results are compared with the magnetic properties of samples obtained through conventional methods, to assess the feasibility of replacing them with additive manufacturing. The novelty of this work is in developing a new understanding of the laser parameters that positively impact the laser powder bed fusion of magnetic components made of Fe-50 wt% Ni alloy.

15.2   Methodology

15.2.1   Sample Fabrication

Commercial Fe-50 wt% Ni alloyed powders were purchased, which were fabricated using Nitrogen atomization, with a particle size < 30 µm. Cylindrical samples were fabricated and built on a stainless steel construction platform, using laser powder bed fusion (Concept Laser Mlab 200R Ge) under a nitrogen atmosphere. The samples were fabricated using a 200 W fibre laser with a spot size of ~75 µm varying the volumetric energy density (VED). Additionally, a meander scanning pattern was employed with a 67° rotation between the consecutive layers. The samples were cylinders of 8 mm in height and 6.4 mm in diameter following ASTM E9 [15]. As shown in Table 15.1, the fabrication followed the design of the experiment (DOE) with variables laser power (P) and laser speed (V), both on three levels, producing each variable set in triplicates. The layer thickness and hatching space were set to 30 µm and 70 µm, respectively. After the fabrication, the as-built samples (AB) were removed from the stainless steel platform using wire electric discharge machining (W-EDM), applying a constant voltage of 100 V and a current of 2.5 A, respectively.

Additionally, an 8 mm in diameter and 50 cm in length Fe-50 wt% Ni bar (abbreviated AR—as-received) was purchased, which was cut with an abrasive disc to produce samples of 6 mm in height.

Table 15.1 Samples fabricated through additive manufacturing and obtained from conventional technology (wrought)

ID	P (W)	L (µm)	V (mm·s^{-1})	H (µm)	VED (J·mm^{-3})
AB S1	180	30	300	70	285.7
AB S2	180	30	400	70	214.3
AB S3	180	30	500	70	171.4
AB S4	190	30	300	70	301.6
AB S5	190	30	400	70	226.2
AB S6	190	30	500	70	181.0
AB S7	200	30	300	70	317.5
AB S8	200	30	400	70	238.1
AB S9	200	30	500	70	190.5
AR	As received or commercial sample				

15.2.2   Microstructural and Density Characterization

The metallographic specimens were prepared by wet grinding using sandpaper from #400 to #4000 grit and then polished with colloidal silica suspension. The microstructure was revealed using an aqua regia, composed of 15 ml HCL and 5 ml HNO_3, for 10 s. The surface images were produced with a scanning electron microscope (SEM) ZEISS 1540XB. The density was measured with the Archimedes method, whose values varied from 8.09 to 8.13 g·cm^{-3}, reaching 98% of relative density.

The phase composition was determined by X-ray diffraction (XRD) using an X'Pert3 MRD XL and equipped with Cu Kα1 radiation source ($\lambda = 1.54056$ Å). The accelerating voltage and current were 40 kV and 40 mA, with a scan rate of $0.02°·s^{-1}$ in a scan range of 20–80°. The phases were identified using X'pert, and then, the Rietveld refinement was performed using MAUD software.

15.2.3   Magnetic Characterization

Next, the saturation magnetization taken at 80,000 A·m^{-1}(B_{80k}) and peak permeability (μ_r) of commercial and additively manufactured cylindrical samples were measured. The magnetizing current was provided by a bespoke hysteresis graph developed at Cardiff University [16] incorporating a Kepco bipolar DC power supply Lakeshore Gaussmeter and Fluxmeter, and a PC running a custom-designed LabVIEW virtual instrument. The sample was wound with a 10-turn coil and magnetized to a peak magnetic field strength of 80 kA·m^{-1} with a cycle time of approximately 5 min.

15.3   Results and Discussions

15.3.1   Morphological Characteristics

Figure 15.1 shows the Fe-50 wt% Ni powder alloy SEM image and its particle size distribution. The particles are mainly spherical, where the bigger particles have some satellites of small diameter, while the rest of the powder is composed of a large number of small particles. The histogram exhibits a log-normal distribution, where 90% of the particles are under 30 μm and many particles are about 5 μm in diameter.

Figure 15.2 shows the SEM image of an as-built sample, taken from the top surface, and its diffraction pattern. The SEM image shows the micrograph of the alloy whose grains are randomly oriented and with grain size distribution due to the fabrication method [17]. The zoom image shows the grain boundary and the structure of fine dendrites inside of the equiaxed grains observed commonly in metallic alloys
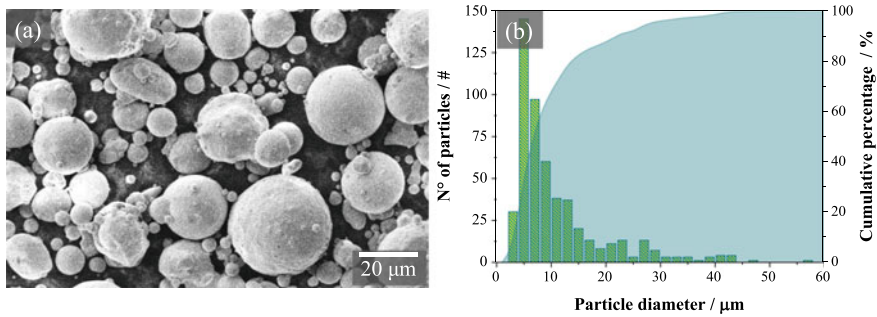
Fig. 15.1 **a** SEM image of alloying powders and **b** histogram of particle size distribution
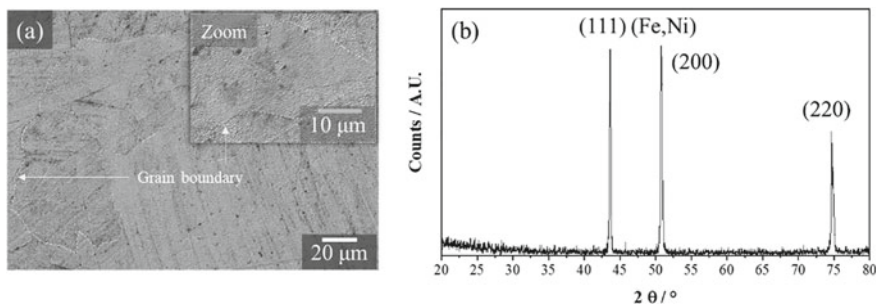

Fig. 15.2 **a** SEM image of AB sample surface and **b** the X-ray sample diffraction pattern collected with Cu Kα radiation

fabricated through AM [18, 19]. It is important to note that small pores (approximately 5 μm) were observed in both the top view and cross-section. However, the density reached was on average 98.4% ± 0.5% as measured by the Archimedes principle.

The diffraction pattern shows peaks associated with the γ-FCC (face-centred cubic) structure with a space group Fm–3 m composed of Fe and Ni atoms. According to the Rietveld refinement, the cubic cell has a lattice parameter of 3.588 Å and suggests texture oriented in (200). F. Haftlang et al. [12] researched the Fe-50% Ni fabricated through direct energy deposition (DED) and the influence of the crystallographic orientation-dependent magnetic properties. They found that maximization of magnetic properties could be done when the grains are oriented on Cube {001} <100> [5].

15.3.2 Magnetic Properties

Figure 15.3 compares the complete hysteresis loops (B–H curves) and zoom of AR and some AB samples. The loops are typical of soft magnet materials, where the AR sample reaches saturation under a small external magnetic strength, reflecting high permeability (μ_r) characteristics. In fact, all AB samples exhibited lower permeability than AR samples due to the internal defects generated by LPBF, which hindered magnetic domain alignment at the same magnetic force applied. However, the magnetic saturation at 80,000 A·m^{-1} (B$_{80\,K}$) was similar between the AR and AB samples whose values were 1.71 ± 0.03 T for AR and a range of 1.56 ± 0.12 T to 1.73 ± 0.09 T for AB. It demonstrated that AB can reach similar values regarding magnetic saturation, whose values seem to depend on the alloy rather than other factors. Table 15.2 shows the principal data extracted from the hysteresis loop.

Similar values have been reported for magnetic saturation [4, 8, 20] but with other fabrication techniques with permeabilities over 40,000 [12]. However, samples fabricated through AM can reach a permeability of 5,000 with a coercivity (H_c) of 100 A·m^{-1} [9] and a magnetic saturation of 1 T [11]. Nonetheless, the AB samples move in a wide range of H_c from 1,730.5 ± 173.8 to 455.5 ± 158.7 A·m^{-1} It is due to the presence of sample's internal defects as porous, voids, residual stress, dislocation density and impurities [4, 19, 21] that impact negatively the magnetic properties. These internal defects are often part of the metallic samples manufactured by AM, which are characterized by having an average of 2% porosity when considered fully dense and the residual stress left by local heating and rapid solidification. Therefore,
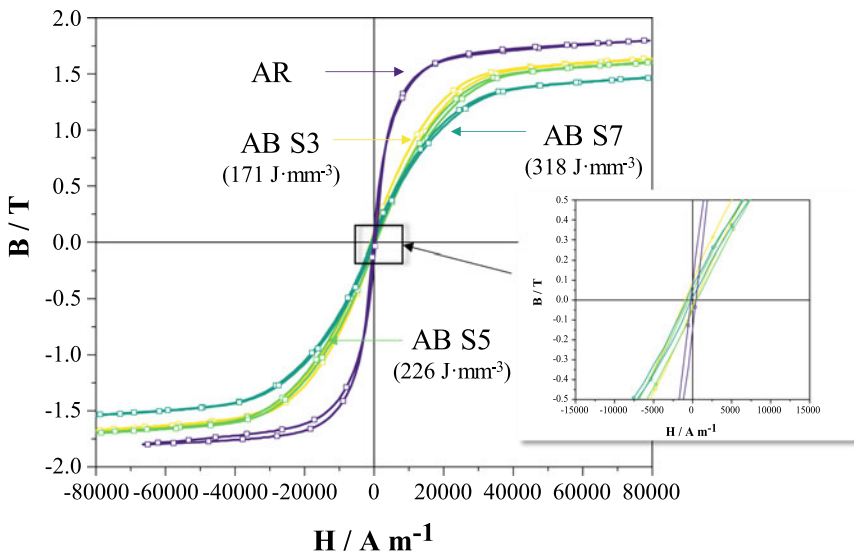

Fig. 15.3 Magnetic hysteresis plot (*B–H* curves) of the magnetic field strength (*H*) and flux density (*B*) of AR and selected AB samples

Table 15.2 Magnetic field saturation, permeability, and coercivity of the as-built and as-received samples

ID	$B_{80\,k}$ (T)	μ_r (-)	H_c (A·m^{-1})
AB S1	1.64 ± 0.02	66.3 ± 0.1	455.5 ± 158.7
AB S2	1.72 ± 0.10	64.4 ± 19.3	1,730.5 ± 173.8
AB S3	1.63 ± 0.01	64.5 ± 1.4	1,390.9 ± 96.3
AB S4	1.73 ± 0.09	62.5 ± 0.1	1,092.1 ± 108.8
AB S5	1.63 ± 0.00	64.3 ± 6.1	978.9 ± 86.3
AB S6	1.63 ± 0.00	59.8 ± 0.7	555.3 ± 447.7
AB S7	1.56 ± 0.12	56.5 ± 3.9	797.6 ± 315.1
AB S8	1.64 ± 0.02	61.2 ± 4.7	965.6 ± 187.6
AB S9	1.64 ± 0.02	56.5 ± 8.1	993.9 ± 55.0
AR	1.71 ± 0.03	159.3 ± 41.2	558.9 ± 106.0

it is expected to achieve lower magnetic properties. However, studies have demonstrated that heat treatments that increase the grain size and allow residual stress relief could improve the magnetic properties of samples fabricated by AM [22, 23].

Figure 15.4 uses a contour graph to show the influences of the laser parameters (power and scan speed) on the magnetic properties such as the magnetic "saturation" ($B_{80\,k}$), the permeability (μ_r), and coercivity (H). The results show that the combination of low laser power and speed is possible to achieve the maximum B_{80k} and μ_r and the lowest coercivity. The latter phenomenon can be attributed to the low laser speed, which enables the melting of the layers while concentrating the power in smaller increments.

Figure 15.5 shows a scatter matrix that combines the magnetic characteristics and the laser parameters utilized in the construction of the samples, providing statistical evidence of their correlation using the Pearson coefficient (r). The VED is strongly influenced by the laser speed (V) rather than the laser power (P) since as the speed increases VED drops drastically. The matrix reveals an inverse relationship between P and μ_r, suggesting that excessive melting of the layers may lead to an increase in microstructural defects. As V increases, there is a corresponding increase in the
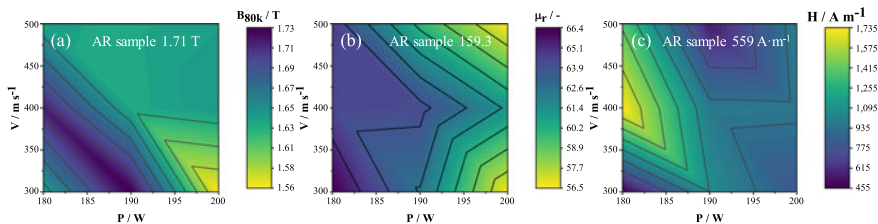

Fig. 15.4 Contour plot of the **a** magnetic field (B) collected at 80 k A·m^{-1}, **b** permeability (μ_r), and **c** coercivity (H) influenced by laser power (P) and scanning speed (V)
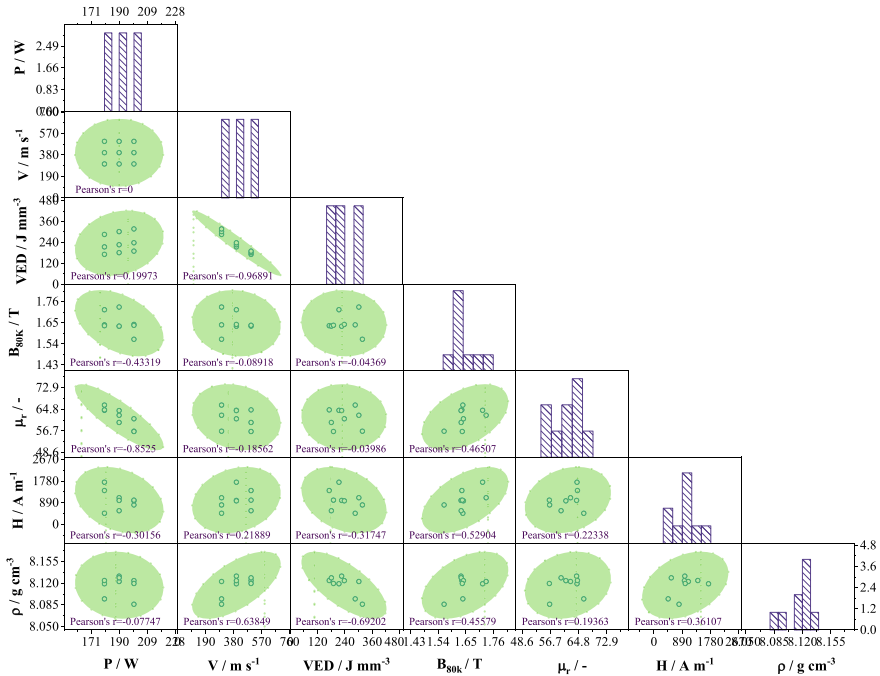
Fig. 15.5 Scatter matrix to visualize bivariate relationships between combinations of laser power and speed, volumetric energy density (VED), sample density (ρ), and magnetic properties

sample density (ρ), which suggests that some magnetic properties can be attributed to the presence of porosity. This is evident in the case of B_{80k} and H, which exhibit a slight positive correlation with density.

15.4 Conclusions

The comparison of the magnetic properties of samples manufactured conventionally and by LPBF, when varying the laser power and speed, indicates the following:

- The B_{80k} achieved for samples produced by LPBF was close to the commercial samples. This means that the magnetic saturation was somewhat unaffected by the type of manufacturing method employed.
- The μ_r is greater in AR samples than AB due to the presence of many internal defects in the last, since this acts as a pinning mechanism for magnetic domain walls. This opens the opportunity to explore the effect of annealing to decrease or eliminate some of these defects to improve the magnetic properties.

- The laser speed affects the volumetric energy, used to construct the AB samples, more than the laser power. Therefore, V influences the permeability, where at higher laser speed, the permeability decreases due to the appearance of more internal defects as porosity.
- The best magnetic properties obtained using AM were achieved using a laser power of 190 W and a low speed of about 300 m·s^{-1}, with total volumetric energy close to 300 J·mm^{-3}.
- The alloy produced through LPBF exhibits magnetic properties that are comparable to those of the same alloy obtained through conventional methods. Therefore, further research is needed to explore the potential of laser powder bed fusion and to manufacture Fe–Ni components.

References

1. Inoue, A., Kong, F.: Soft magnetic materials. In: Encyclopedia of Smart Materials. Elsevier, pp 10–23 (2022)
2. Azuma, D.: Magnetic materials. Wide Band. Pow. Semicond. Pack.: Mat., Comp. Reliab., 97–107 (2018). https://doi.org/10.1016/B978-0-08-102094-4.00005-0
3. Collocott, S.J.: Magnetic materials: domestic applications. In: Reference Module in Materials Science and Materials Engineering. Elsevier (2016)
4. Shokrollahi, H., Janghorban, K.: Soft magnetic composite materials (SMCs). J. Mater. Process. Technol. **189**, 1–12 (2007). https://doi.org/10.1016/j.jmatprotec.2007.02.034
5. McHenry, M.E., Laughlin, D.E.: Magnetic Properties of Metals and Alloys. Elsevier, Fifth Edit (2014)
6. Fathabad, S.M., Shahri, F., Gholamipour, R.: The microstructural characterization, physical and dynamic magnetic properties of (Ni49Fe51)100-xCrx (x = 0,3,7) thin sheets. Metall. Mater. Trans. A Phys. Metall. Mater. Sci. **51**, 323–330 (2020). https://doi.org/10.1007/s11661-019-05504-6
7. Bernier, F., Ibrahim, M., Mihai, M., et al.: Additive manufacturing of soft and hard magnetic materials used in electrical machines. Met. Powder Rep. **75**, 334–343 (2020). https://doi.org/10.1016/j.mprp.2019.12.002
8. Ma, J., Qin, M., Zhang, L., et al.: Microstructure and magnetic properties of Fe-50%Ni alloy fabricated by powder injection molding. J. Magn. Magn. Mater. **329**, 24–29 (2013). https://doi.org/10.1016/j.jmmm.2012.10.019
9. Mazeeva, A.K., Staritsyn, M.V., Bobyr, V.V., et al.: Magnetic properties of Fe–Ni permalloy produced by selective laser melting. J. Alloys Compd. **814**, 152315 (2020). https://doi.org/10.1016/j.jallcom.2019.152315
10. Yakout, M., Elbestawi, M.A., Wang, L., Muizelaar, R.: Selective laser melting of soft magnetic alloys for automotive applications. In: The 6th Joint Special Interest Group meeting between euspen and ASPE: Advancing Precision in Additive Manufacturing, 1–4 (2019)
11. Kim, E.S., Haftlang, F., Ahn, S.Y., et al.: Mechanical and magnetic properties of soft magnetic Fe–Ni permalloy produced by directed energy deposition processes. J. Mater. Sci. **57**, 17967–17983 (2022). https://doi.org/10.1007/s10853-022-07110-1

12. Haftlang, F., Kim, E.S., Kim, H.S.: Crystallographic-orientation-dependent magnetic properties of Fe–Ni permalloy in-situ alloyed using additive manufacturing. J. Mater. Process. Technol. **309**, 117733 (2022). https://doi.org/10.1016/j.jmatprotec.2022.117733

13. Tsakiris, V., Petrescu, M.: Influence of purity and fabrication technology on the properties of soft magnetic Fe-50Ni alloy. UPB Scient. Bull. Series B: Chem. Mat. Sci. **69**, 67–78 (2007). https://doi.org/10.13140/2.1.3045.0564

14. Zhang, B., Fenineche, N.E., Zhu, L., et al.: Studies of magnetic properties of permalloy (Fe30%Ni) prepared by SLM technology. J. Magn. Magn. Mater. **324**, 495–500 (2012). https://doi.org/10.1016/j.jmmm.2011.08.030

15. ASTM Standard E9-09: Standard test methods of compression testing of metallic materials at room temperature. Ann. Book of ASTM Stand. **3**(1), 92–100 (2012)

16. Anderson, P.: A universal DC characterisation system for hard and soft magnetic materials. J. Mag. Mag. Mater **320** (2008). https://doi.org/10.1016/j.jmmm.2008.04.034

17. Akram, J., Chalavadi, P., Pal, D., Stucker, B.: Understanding grain evolution in additive manufacturing through modeling. Addit. Manuf. **21**, 255–268 (2018). https://doi.org/10.1016/j.addma.2018.03.021

18. Joshy, J., Kuriachen, B.: Influence of heat-treatment and cryo-treatment on high temperature wear performance of LPBF Inconel 718. Wear, 204681 (2023). https://doi.org/10.1016/j.wear.2023.204681

19. Yang, J., Zhu, Q., Wang, Z., et al.: Effects of metallurgical defects on magnetic properties of SLM NiFeMo permalloy. Mater Charact **197**, 112672 (2023). https://doi.org/10.1016/j.matchar.2023.112672

20. Fiorillo F (2004) Soft Magnetic Materials. In: Characterization and Measurement of Magnetic Materials. Elsevier, pp 25–88

21. Lamichhane, T.N., Sethuraman, L., Dalagan, A., et al.: Additive manufacturing of soft magnets for electrical machines—a review. Mat. Today Phys. **15**, 100255 (2020). https://doi.org/10.1016/j.mtphys.2020.100255

22. Yin, Q., Ma, Y., Chen, G., et al.: Electron beam welding with in situ heat treatment: An effective method for optimization of soft magnetic properties of permalloy. J. Manuf. Process. **77**, 642–651 (2022). https://doi.org/10.1016/j.jmapro.2022.03.042

23. Alves, E.M.M., Silveira, C.C., da Cunha, M.A.: Influence of stress relief annealing temperature on the cutting edge microstructure and on the recovery of magnetic properties of grain oriented electrical steel. Mater Charact **166**, 110408 (2020). https://doi.org/10.1016/j.matchar.2020.110408